ELSEVIER

Chemical Engineering Journal 137 (2008) 144–153

Chemical Engineering Journal

www.elsevier.com/locate/cej

Stimulated in vitro bone-like apatite formation by a novel laser processing technique

Emilia Pecheva [a,*], Todor Petrov [a], Cristian Lungu [b,1], Paul Montgomery [c,2], Lilyana Pramatarova [a]

[a] *Institute of Solid State Physics, Bulgarian Academy of Sciences, 72 Tzarigradsko Chaussee blvd., 1784 Sofia, Bulgaria*
[b] *National Institute for Lasers, Plasma and Radiation Physics, 409 Atomistilor Str., 77105 Bucharest-Magurele, Romania*
[c] *Institut d'Electronique du Solide et des Systèmes (InESS), UMR 7163, 23 rue du Loess, 67037 Strasbourg, France*

Received 18 May 2007; received in revised form 27 July 2007; accepted 31 July 2007

Abstract

Hydroxyapatite is a mineral widely studied as an artificial replacement material in dentistry and medicine due to its chemical and crystallographic resemblance to bone and tooth minerals. New trend of stimulating the hydroxyapatite formation in vitro has evolved by applying various sources of external energy. Lasers have been widely used in biomaterials area as clean and powerful sources of energy and have diverse bioapplications. They are excellent tools for creating micrometer-scale structures by precise and flexible irradiation of small and complex shapes. Using a hierarchical approach that mimics the natural material formation processes, we developed a method to produce materials with controlled physical structure at both micro- and nanometer scale. Materials organized on multiple length scales bear a closer resemblance to biological matrices than those with single scale features, and thus materials with multi-scale organization should be more advantageous in biomedical applications. In the applied laser–liquid–solid interaction method, micrometer scale architecture with precisely controlled size and shape is induced by laser irradiation of various surfaces and then nanostructured hydroxyapatite is grown preferably on the micrometer-sized areas by a biomimetic approach. The method results in an enhanced calcium phosphate formation on the materials' surfaces which further facilitates the growth of a thicker hydroxyapatite layer. In this work we present our method and the application of optical emission spectroscopy for the in situ monitoring of the processes during the laser–liquid–solid interaction. Furthermore, tests with osteoblast-like cells reveal the biocompatibility of the hydroxyapatite layers obtained as a result of the laser–liquid–solid interaction method.

Keywords: Bone-like apatite; Hydroxyapatite; Synthesis; Stimulated growth; Laser processing; Nanostructured surfaces; Porous materials; Optical diagnostics

1. Introduction

Hydroxyapatite (HA, chemical formula $Ca_{10}(PO_4)_6(OH)_2$) is widely studied as an artificial bone and teeth replacement material in dental and orthopedic implants, as coating of hard tissue implants, bone fillers, and for drug delivery, due to its chemical and crystallographic resemblance to bone and tooth minerals [1]. HA is known to have an appropriate biological activity when implanted in living organisms and this property has attracted growing interest in the last decades. The goal of the biomaterials synthesis and processing nowadays is to mimic the way materials have been created in nature. Organisms in nature create perfect fine mineralized structures with diverse biological functions and very often from simple salt solutions through interactions between inorganic and organic substances [2,3]. Stimulated by fascinating natural examples, such as bones, teeth, cartilage, shells and corals, attempts are being made to develop synthetic, biomimetic nanocomposites by simulating the basic principles of biomineralization. Following this goal, many researchers have been exploring the potential of a simple immersion method in an aqueous supersaturated solution, known as simulated body fluid (SBF) [4] in order to mimic the process of biological apatite formation. A disadvantage of the method is the long time required to produce calcium phosphate (CaP) coatings. Therefore, a new trend of applying external energy to stimulate the HA formation in vitro has evolved: ultrasound and electrical field, ultraviolet and microwave irradiation have been used with this purpose [5–7]. Fang et al. [5] applied

* Corresponding author. Tel.: +359 2 9795000x265; fax: +359 2 9753632.
E-mail address: emily@issp.bas.bg (E. Pecheva).
[1] Tel.: +40 21 4574550; fax: +40 21 4574468.
[2] Tel.: +33 3 88106231; fax: +33 3 88106548.

1385-8947/$ – see front matter © 2007 Elsevier B.V. All rights reserved.
doi:10.1016/j.cej.2007.07.096

ultrasound to accelerate the formation of HA in aqueous solutions at low temperature and managed to reduce the time for the HA formation from hours to minutes. Another research group [6] reported the formation of bio-resembling apatite crystals from SBF on TiO_2 under illumination with ultraviolet light and following soaking of the samples for 10 days in the SBF. There is also a tendency of using microwave energy for acceleration of specific chemical reactions [7]; under the microwave influence, precipitation of HA from aqueous medium was obtained within an hour. Recently, a novel method involving laser–liquid–solid interaction (LLSI) for the facilitated synthesis of HA by using a laser irradiation of materials simultaneously immersed in the supersaturated SBF has been proposed [8–13].

The idea of using laser light was based on the fact that over the past two decades, laser sources of energy have proved to be major tools for surface processing of large variety of metals, ceramics and polymers, as well as for processing of living tissues and synthesis of biocompatible materials. Lasers have been utilized as exceptional contactless, fully adaptable sources of clean energy. Bioapplications, such as pulsed laser deposition and processing of HA [14,15], biofilms modification [16], bone defect healing [17], modification of root canal dentine [18], laser sterilization of dental implants [19] are already well established. Lasers have also been employed to increase the long-time performance of Ti dental implants through assuring cleanness, specific microrelief and stable oxide layer on the surfaces [20]. Particularly, pulsed lasers have unique qualities that can be applied to process biomaterial thin films. Pulsed lasers have proven to be an invaluable tool in the research and development of new thin film materials because of the unique nature of the laser-material interaction.

The proposed in our work method of LLSI was based on the simultaneous interaction between a scanning pulsed laser beam and a liquid precursor solution (SBF or distilled water as a control solution) in the presence of a solid substrate [8–13]. We used metal, semiconductor and insulator as substrates. Metals (Ti, Ti alloys, Co–Cr–Mo alloys, austenitic stainless steels, tantalum and zirconium) are most frequently used for implants [21–23]; they form protective nm-thick native oxide layer on their surfaces which determine their excellent corrosion resistance and decreases the leaching of metal ions from the implant surface. These properties make metal materials appropriate for implantation in the human body. Silicon (Si) is one of the most abundant elements on earth, and it is also present in the human blood plasma in the form of orthosilicic acid [$Si(OH)_4$] which is vital for the optimum growth and development of bones and collagen in the living organism [24]. Glasses are rich in SiO_2 which yields the formation of surface Si-OH^- groups in the SBF, which on their turn ensure active sites for the formation of HA [25]. Further, porous and nanostructured materials (porous Si, polycrystalline Si and CdSe/SiO_x nanostructures), obtained by using well-established nanotechnologies were also utilized in our work, since nanosized objects, as well as porous structures are known to promote bone and tissue ingrowth into open pores and they also allow to be easily biodegraded and bioresorbed [24,26–31].

Materials structural properties at micro-and nanometer scale influence the cellular responses [27,28]. It has been shown that materials organized on multiple length scales bear a closer resemblance to biological matrices than those with single scale features, and thus materials with multi-scale organization should be more advantageous in biomedical applications [27,28]. Using an approach that mimics the natural material formation processes, the method of LLSI was utilized to produce materials with controlled physical structure at both micro- and nanometer scale. By applying this process, various microdesigns can be realized on the material surface by a precise scanning system. The LLSI results in an enhanced CaP formation on the material surface, compared to the traditional method of prolonged soaking in SBF, and this result is attained as a single one-step and time-sparing process. The new laser processing method can yield a significant progress in the materials coating with bone-like apatite in terms of nucleation rate, simplicity and availability to coat complex shapes. It is carried out under a room temperature and atmospheric pressure, i.e. it does not require the presence of buffer gasses or vacuum conditions. However, the mechanisms of the enhanced CaP formation are not clear enough. Observation of the interaction of the laser beam with the substrates immersed in the solution by an optical diagnostic technique was expected to give us more details on the mechanisms of the LLSI process. For this purpose we used optical emission spectroscopy (OES) as a plasma diagnostic tool for in situ monitoring during the LLSI process. The technique was used to observe the emission from excited species and was applied for a first time in such a complex interaction like 'laser light–solution–solid substrate'.

Materials, compatible with cells are important in medical applications and therefore the interactions of the cells with the materials have been intensively investigated [32]. Cells are highly sensitive to topography, roughness, chemistry, surface charge, and hardness [33,34]. Cell–material interactions in vitro may be approximated by the process of cell adhesion and spreading, which is a convenient way to determine the biocompatibility of a material. In our study, the CaP layer grown on glass substrates by applying the LLSI process was tested in terms of its cell compatibility with osteoblast-like cells.

2. Experimental

2.1. Materials

2.1.1. Stainless steel, silicon, silica glass

Samples from stainless steel AISI 316 (further named SS), *n*-type silicon with (1 0 0) orientation (named S), and silica glass Herasil (named SG) subjected to standard mechanical treatment [35] were prepared. All samples were subjected to LLSI process and subsequent soaking in the SBF solution at 37 °C for up to 24 h. One group of samples was taken out of the SBF immediately after the end of the LLSI in order to study the instantaneous effect of the laser irradiation. In both cases, the samples were finally washed with distilled water and dried in air before investigations.

2.1.2. CdSe/SiO_x nanostructures

CdSe/SiO_x nanostructures were prepared by multi-step sequential evaporation of SiO and CdSe layers (each having

thickness of up to 10 nm) on rotated Corning glass substrates under a vacuum of 10^{-3} Pa [35]. Thus, 2D distribution of CdSe nanoparticles in the SiO_x layer was obtained and they were in contact with each other, thus forming structure of the type superlattice. The total thickness of the CdSe/SiO_x multi-layer structures obtained was 320 nm. Nanostructured samples were subjected to LLSI process and subsequent soaking in the SBF solution at 37 °C for 18 h, and after the soaking they were washed with distilled water and dried in air.

2.1.3. Porous Si

Porous Si (PS) layers were formed on Si substrates by electrochemical etching in a mixture of HF:C_2H_5OH:H_2O = 2:1:1 and illumination with 500 W halogen lamp [35,36]. Thickness of the obtained PS layers was in the range of 1–40 μm. According to the proposed in [36] model, the surface of the PS consisted of Si crystals with a few nm in dimensions, covered by a thin suboxide (SiO_x) layer containing C, O, H and OH. As-prepared samples were subjected to LLSI process and subsequent soaking in the SBF solution at 37 °C for 15 h, and after the soaking they were washed with distilled water and dried in air.

2.1.4. Polycrystalline Si

Glass substrates were coated subsequently with Al and amorphous Si (a-Si) by radio-frequency magnetron sputtering from an Al target in Ar atmosphere (0.5 Pa) at room temperature [37]. The thickness of the Al and a-Si layers was about 100 nm. The layers were then isothermally annealed in air, vacuum or $N_2 + H_2$ (forming gas) to obtain the polycrystalline Si (poly-Si) layers. Further, the samples were subjected to LLSI process and after subsequent soaking in the SBF solution at 37 °C for 4 h they were washed with distilled water and dried in air.

2.2. HA growth from liquid precursor solution (SBF)

SBF is an inorganic aqueous solution that resembles the ion composition, concentrations and pH of the human blood plasma. Two base solutions were prepared by reagent-grade chemicals. The first one consisted of NaCl (15.99 g/l), KCl (0.45 g/l), $CaCl_2$–$2H_2O$ (0.74 g/l) and $MgCl_2$–$6H_2O$ (0.61 g/l) dissolved in 1 l of distilled water. The second one included Na_2SO_4–$10H_2O$ (0.32 g/l), $NaHCO_3$ (0.71 g/l) and K_2HPO_4–$3H_2O$ (0.69 g/l) dissolved in 1 l of distilled water. The pH of the two solutions was buffered at pH 7.4 with Tris–hydroxymethyl–aminomethane buffer or hydrochloric acid [4]. Separately stored, the two solutions do not yield precipitation. Before immersion of the samples, equal quantities of the two base solutions were mixed to give the final SBF solution. It has to be noted that NaCl constitutes 80% of the salts dissolved in the precursor solution.

2.3. Set-up for LLSI method

The experimental set-up included an open deposition system where the solution was placed in a reaction glass container and the solution temperature was controlled by a thermostat (Fig. 1). The substrates were immersed one by one on the bottom of the container with 50 ml of the solution (layer thickness above the samples was 20 mm) at room temperature and simultaneously irradiated by a laser. CuBr pulsed vapor laser (λ = 578.2 nm, laser energy per pulse 1.2 kW, laser power density 60 MW/cm^2, pulse duration of 30 ns, pulse repetition rate 19 kHz, velocity of the scanner 1000 mm/s, laser beam diameter in the focal plane 50 μm) was used in the experiment. The laser beam was directed perpendicularly to and focused on the substrate surface through the solution. By means of a scanning system, a surface pattern of seven concentric squares, each separated by a distance of 200 μm was formed at the edges of each sample as seen in the upper left corner of Fig. 1, and the middle of the samples was not irradiated. The interaction time of the laser beam with each sample was less than 5 min. After the irradiation all samples were subsequently immersed in 500 ml total volume of irradiated SBF for up to 24 h under physiological conditions (37 °C, pH 7.4). Before investigations, all samples were washed with distilled water and dried in air. The laser applied in our work is technologically available and well established, and it has been chosen also due to its possibility for precise and flexible irradiation of small and complex shapes peculiar to many implants, as well as for its high power density.

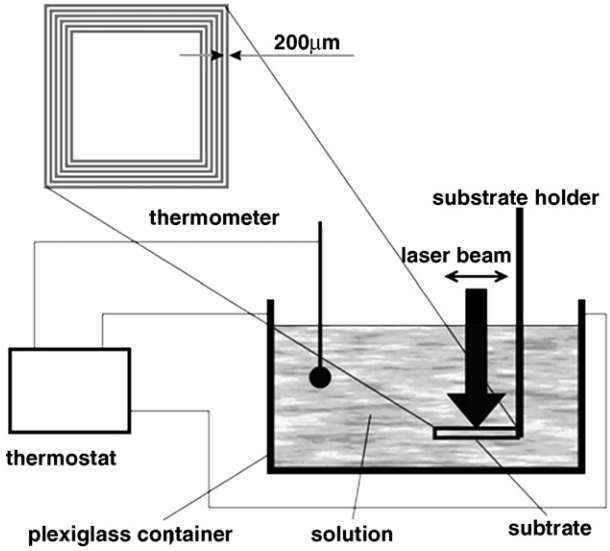

Fig. 1. The set-up used in the LLSI process and design of the laser irradiation (upper left corner).

2.4. Biocompatibility test with osteoblast cell cultures

In vitro biocompatibility of the CaP layers grown on laser-treated and non-treated glass samples with osteoblast-like cells (MG-63, concentration of 125,000 cells/cm^2) was examined. The cells were cultured in Dulbecco's modified Eagle medium supplemented with 10% fetal calf serum and 0.5% antibiotics, incubated at 37 °C and 5% CO_2 for 1, 3, 5, and 7 days.

2.5. Analyses

Scanning electron microscope (SEM; JSM-25 SIII) and optical reflection microscope (Olympus BX40) were used to

characterize the layers grown on all materials after the LLSI process. The elemental composition of the layers was measured by energy dispersive X-ray spectroscopy (EDX; JEOL JSM-840). The layer structure was studied by Raman spectroscopy (Jobin Yvon Horiba micro-spectrometer; $\lambda = 532.14$ nm) and X-ray diffraction (XRD Siemens D5000, Bruker GmbH, Germany, $\lambda = 1.54$ Å, $2\theta = 20$–60°, step size of $\Delta 2\theta = 0.1^\circ$; JCPDS file No 09–432). Absorption of SBF was measured with μ-Quant spectrometer (range of 200–1000 nm). Ca and P concentrations in the SBF were investigated by inductively coupled plasma mass spectrometry and ion chromatography. Roughness and height profiles were estimated by coherence probe microscopy (CPM; Leitz microscope (Wetzlar) with Linnik objective of 50×, $\lambda = 350$–1100 nm, dynamic range 100 μm, axial and lateral resolution of 10 nm and 0.45 μm, respectively).

Optical diagnostic was carried out by OES in the SBF. Doubly distilled water was used as a control solution. After each irradiation, the solution (SBF or water) in the reaction container was changed in order to reduce the influence of particles ablated from the materials on the detected signal. The direction of the observation of the emitted light was chosen to be perpendicular with respect to the laser beam axis as shown in Fig. 2. The image plane of the expanding plasma was scanned with 1 mm step by the entrance slit of an optical fiber mounted on a 3D stage. Then the emission light was directed onto the entrance slit of a SM-242 CCD spectrometer (CVI Laser Optics) by the optical fiber. The spectrograph (crossed Czerny-Turner type) had an F/2.7 aperture and 1200 grooves/mm holographic grating. The emission spectra of the plasma were measured by a linear CCD sensor array and recorded by an optical multi-channel analyzer (range of 200–900 nm, spectral resolution 1.5 nm). Light emission was accumulated for 50–7 s because the processes analyzed in this experiment were stable within this time scale.

Cell morphology was observed by SEM (JEOL 5400 LV) after a standard procedure for cell preparation. Cell viability was evaluated by the Trypan Blue exclusion test. A Kruskal–Wallis nonparametric test was performed for statistical analysis ($p < 0.05$ was considered statistically significant). The overall cell morphology was observed using a laser scanning confocal microscope (LSCM; LSM 510, Zeiss, magnification 10×).

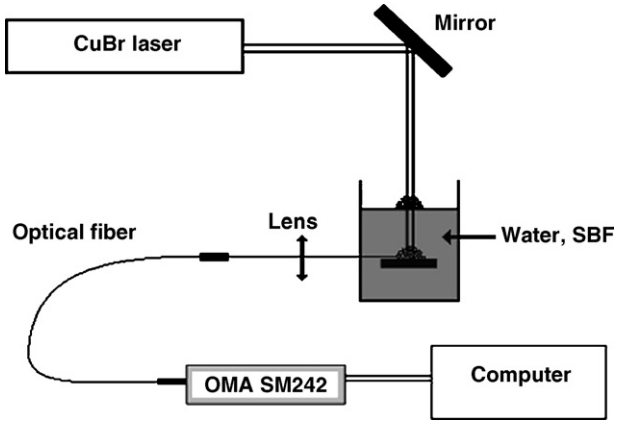

Fig. 2. Scheme showing the LLSI set-up joined with the system for optical diagnostic of laser plasma used for the in situ monitoring of the processes during the LLSI.

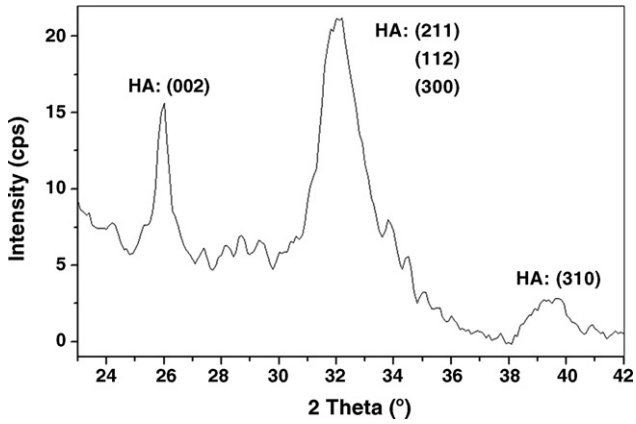

Fig. 3. XRD spectrum typical for the HA obtained after the LLSI process and subsequent soaking in the SBF of the various surfaces used in our work.

3. Results and discussion

3.1. HA formation through LLSI process

X-ray diffractogram typical for the HA was recorded from the layers grown on the various surfaces (SS, S, SG materials, CdSe/SiO_x nanostructure, PS and poly-Si layers) by applying the LLSI process and it is shown in Fig. 3. The spectrum revealed the formation of non-stoichiometric HA layers by the peaks characteristic of HA: (0 0 2) peak at $2\theta = 26^\circ$ and a broad one centered at 32°, which was an envelope of three overlapping crystalline spacings, namely (2 1 1), (1 1 2) and (3 0 0). The isolated (0 0 2) peak was used to calculate the grain size by using the Scherer formula and it was found that the HA crystals have nanometer dimensions (for all samples less than 100 nm) as in natural apatites [1].

Fig. 4 shows the surfaces of the various materials used in our work, after the LLSI process has been applied in the SBF precursor solution. Control samples of SS, S and SG were taken out immediately after the end of the laser irradiation. Optical reflection microscopy image (Fig. 4a) depicts the laser lines on the S surface and a predominant formation of white particles in the irradiated area. The EDX, Raman and FTIR spectra discussed in [35] revealed the formation of CaP. After subsequent soaking in the SBF solution for 2 h, the number of the white particles in the laser areas, as well as in the non-irradiated samples' center increased. Increasing the time for subsequent soaking yielded quick cover of SS, SG and in a lower degree of the S surface with a white layer, identified by FTIR and Raman spectroscopy as carbonate-containing HA [35]. Layer thickness was evaluated from the FTIR spectra of SS, S and SG materials based on the Beer–Lambert law for the optical density [35]. The layer obtained after LLSI and subsequent soaking was thicker than a HA layer grown on soaked samples (i.e. not subjected to the LLSI process before the soaking). Details of the SS surface after the end of the laser irradiation (Fig. 4b) showed CaP particles, as well as dendrite formations composed of NaCl crystals. In

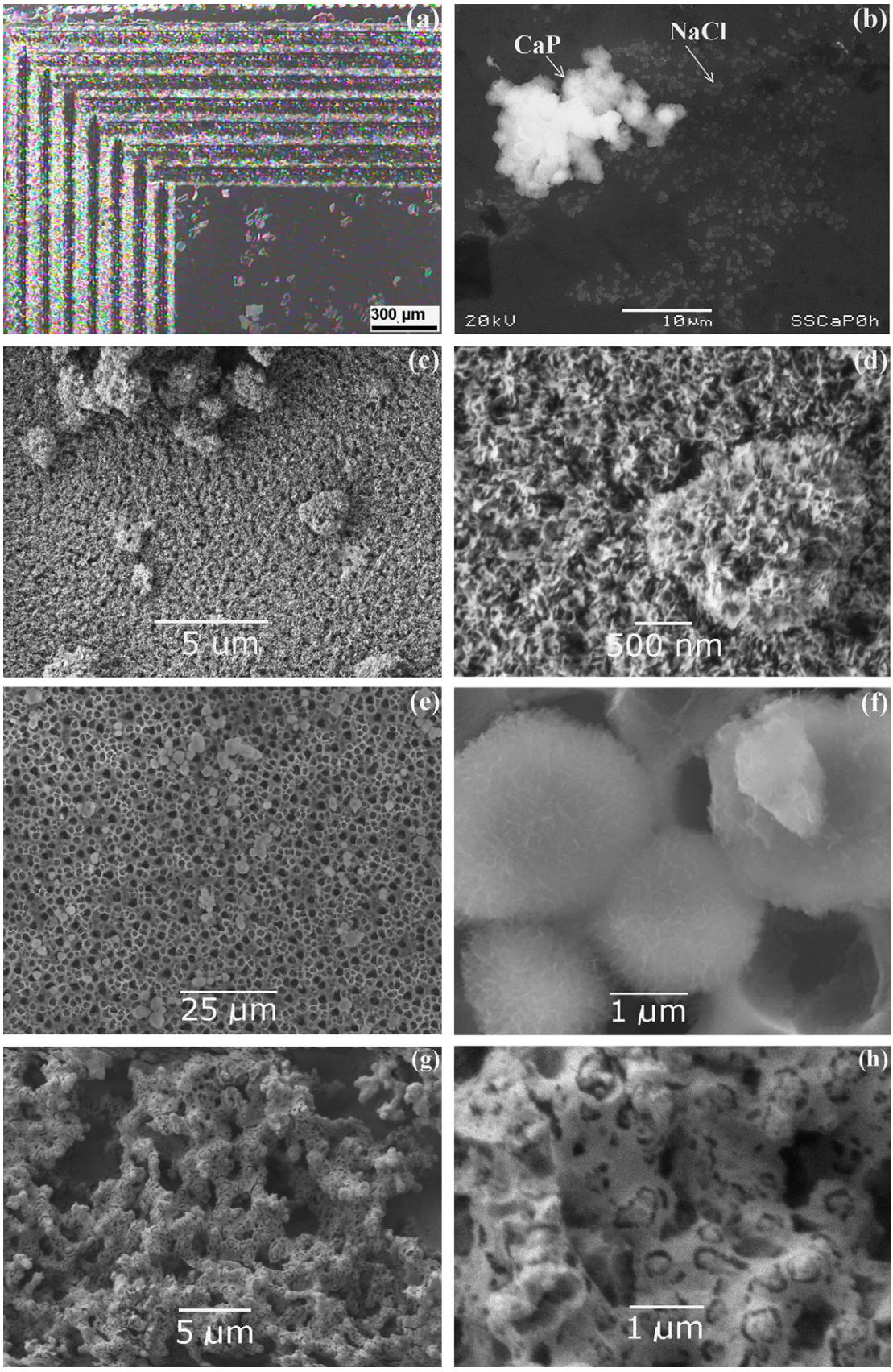

Fig. 4. Surfaces of the various materials used in our work after the LLSI process: (a) optical reflection microscope image of the Si surface taken out immediately after the end of the laser irradiation and (b) details of the steel surface revealed by SEM; (c and d) SEM image of the CdSe/SiO_x nanostructure after the LLSI and subsequent soaking in the SBF for 18 h; (e and f) SEM image of the PS layer after the LLSI and subsequent soaking for 15 h; (g and h) SEM image of the poly-Si layer after the LLSI and subsequent soaking for 4 h.

the SBF solution NaCl salt constitutes 80% of the salts. After dissolving all salts in distilled water, HCl was used to adjust the solution pH. Adding HCl to an aqueous solution in which NaCl salt is dissolved according to the reaction:

$$NaCl\ \ (solid) \Leftrightarrow Na^{+}\ \ (aqueous) + Cl^{-}\ \ (aqueous),$$

drives the equilibrium of this reaction back, and as a result solid NaCl crystallizes [38]. Probably stable CaP nuclei formed due to the applied laser energy and they allowed the enhanced formation of the CaP particles within the laser irradiation time (a few minutes). These particles further facilitated the growth of a thicker HA layer. Such fast CaP formation was not observed when the samples were simply soaked in the SBF [35]. Regarding the pulsed laser irradiation of the materials, there are many experiments described in the literature in which laser irradiation is utilized in a solution of soluble precursors, with different wavelengths, with or without a substrate, and the aim has been to form nanoparticles or to grow nanoparticle layers [39–43]. In our experiments, we obtained enhanced CaP formation on various types of surfaces as a result of the laser irradiation.

On one hand, there was the aqueous SBF solution, participating in the LLSI process. It is known that water is transparent for the visible light such as the one of the CuBr laser used in the experiments (578.2 nm). Absorption of the laser energy in the solution could appear because of the dissolved salts (K_2HPO_4–$3H_2O$, $NaHCO_3$, Na_2SO_4–$10H_2O$, $CaCl_2$–$6H_2O$, $MgCl_2$–$6H_2O$, NaCl, KCl) and the water. The light absorption of freshly prepared SBF and of the two base solutions used in the SBF preparation was measured in the range of 200–1000 nm and no absorption peaks were observed. Measured Ca and P concentrations of freshly prepared SBF showed a considerable decrease after the laser irradiation: fresh SBF had 136 mg/l Ca and 235 mg/l P and after the irradiation the concentrations decreased to 68 mg/l and 82 mg/l, respectively. It is known that when a precipitation begins in a supersaturated solution the ion concentrations decrease [44]. Thus, it was confirmed that the laser irradiation in the LLSI process resulted in the formation of CaP particles. The higher decrease of the P concentration indicated that it was preferentially consumed which can explain the low Ca:P ratio obtained by EDX (Ca:P < 1.0).

Further, CdSe/SiO_x nanostructures were subjected to the LLSI process and the samples morphology after the end of the LLSI and subsequent soaking in the SBF for 18 h is featured in Fig. 4c and d. Dense, sponge-like layer of randomly oriented needle-like crystals with attached crystal aggregates atop covered the nanostructured surface. The layer structure was identified as carbonate-containing HA with inclusion of K, Cl, Na and Mg ions [35]. Natural apatite contains carbonate (CO_3), small amounts of Na, Mg, K, Cl and other elements, it is non-stoichiometric, low crystalline and has a crystal size less than 200 nm [1,45,46]. All these properties ensure a higher extent of dissolution than crystalline commercial HA ceramics, which is desirable when a material coated with synthetic apatite is used as implant in the human body. EDX results showed the presence of Ca, P, O, Si, Cd and Se in the HA layer, minor amounts of Mg and Na, and a higher P than Ca concentration, which led again to Ca:P ratio lower than 1.0 [35]. The stripes of the laser irradiation were clearly visible and allowed measurement of the Ca and P concentration in two specific areas. Higher value was obtained in the case of measurement in the laser-irradiated area (0.76) than out of this area (0.50). This result indicated the predominant attachment of Ca and P under the influence of the laser irradiation. It was assumed that optical stimulation of the photosensitive CdSe was responsible for the higher concentrations of Ca and P in the laser area. CdSe in the prepared samples had an optical bandgap of about 2.0 eV. On illumination with intense laser radiation (power density of 60 MW/cm^2 and $\lambda = 578.2$ nm is equal to 2.2 eV), electron-hole pairs are photogenerated in the CdSe layers of the CdSe/SiO_x structure. It is known that when photoexcited carriers are captured by structural defects they can charge them (if neutral) or cause secondary ionization [47]. This charge possibly stimulated the predominant attachment of Ca and P ions from the SBF to the irradiated areas which further facilitated the HA growth.

As discussed, porous layers are known to promote bone and tissue ingrowth into open pores, and thus allow faster returning to the natural physiological functioning of the living organism [24,26–31]. Recently, PS has been studied as a biomaterial scaffold for the deposition of CaPs, whereby bioactivity can be explicitly induced and applications of such materials include drug delivery, sensing, etc. [11,29,48]. It was found that PS may be tailored to be bioactive and biocompatible material, and thus it is suitable for implantation into a living organism. Some researchers have explored the PS as biodegradable material for slow release of trace elements or drugs and for studying of surface-protein interactions [31,49]. PS has also received considerable interest for applications in medicine due to its solubility in physiologic fluids [24]. On the other hand, PS presents an advantage over other bioactive materials because it is compatible with Si-integrated circuit technology and thus, biosensor devices can be produced to be linked to biological systems. Other advantages of the PS include its high surface-volume ratio, pore size close to the one in nature and high degree of porosity on nanolevel; it is also shown that the semiconductor surface in biomedicine is a prerequisite for preventing the formation of blood curling [50]. In our experiment, the application of the LLSI process on the PS layers and subsequent soaking in the SBF solution for 15 h resulted in the formation of a thin HA layer with sphere-like aggregates of HA crystals partly filling the pores (Fig. 4e and f). EDX measurements showed a decrease of the Ca:P ratio from 0.63 in the laser area to 0.40 in the non-irradiated areas which revealed the stimulating effect of the laser irradiation.

Finally, HA formation was induced by applying the method of LLSI and subsequent soaking in the SBF for 4 h on the poly-Si layers as revealed by XRD, FTIR and Raman spectra [51]. Fig. 4g and h features the porous sponge-like CO_3-containing HA grown on the poly-Si surfaces. Enhancement of the HA growth was observed due to the applied LLSI process as shown in the characteristic Raman spectra in Fig. 5, measured in and out of the laser-irradiated areas. Similar result was observed in the spectra recorded from the HA layers grown by the LLSI on the SS, S, SG materials, as well as on the CdSe/SiO_x nanostructures and the PS layers. Vibrations due to the ν_1 P–O stretching

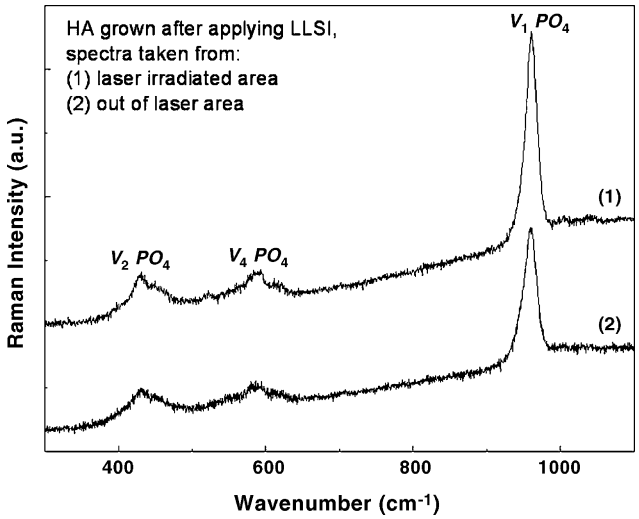

Fig. 5. Raman spectra typical for the HA layer grown on the various materials after applying the LLSI process: spectra recorded from the laser area (1) and out of it (2) revealed the enhancement of the HA growth due to the laser irradiation.

(the strongest peak at 960/cm), ν_2 and ν_4 P–O bending vibrations in PO_4 (at 430 and 590/cm) were present. The intensity of the ν_1 P–O stretching mode was higher when taken from the laser-irradiated area (spectrum 1) than when measured out of it (spectrum 2), thus indicating an enhancement of the HA growth by the applied laser energy.

3.2. In vitro test with osteoblast-like cells

In vitro biocompatibility of the HA layers grown after 6 h on glass samples by (a) LLSI process and subsequent soaking in the SBF, and (b) simple soaking in the SBF, was examined with osteoblast-like cells MG-63 for 1, 3, 5, and 7 days. The test revealed good cell adhesion and spreading on both laser-treated and non-treated samples after 1 and 3 days. However, as can be seen in Fig. 6a, more cells were observed after 1 day on the laser-treated, in comparison to the non-treated samples where the cells did not completely cover the underlying substrate (Fig. 6c). The cell number on both types of surfaces increased after 3 days and they formed a confluent monolayer (Figs. 6b and d) with no specific cell orientation. Proliferation results (Fig. 7) showed a permanent increase of the cell number on the two groups of samples with increasing of incubation time. The increase was more stable on the laser-treated samples (graph 1). After 7 days of cell culturing, these samples showed the highest cell number. A slower increase in the cell number which finally resulted in a lower cell number was observed for the non-treated samples (graph 2). Toxicity tests showed viability of the cells on the CaP grown on laser-treated samples of over 95%. No difference from this value was observed for the layer obtained without a laser irradiation. LSCM images (Fig. 8) revealed that the cells cultivated for 2 h on the HA layer after the LLSI and subsequent soaking for 6 h (left image) were slightly flatter than on the HA grown on the simply soaked samples (right image).

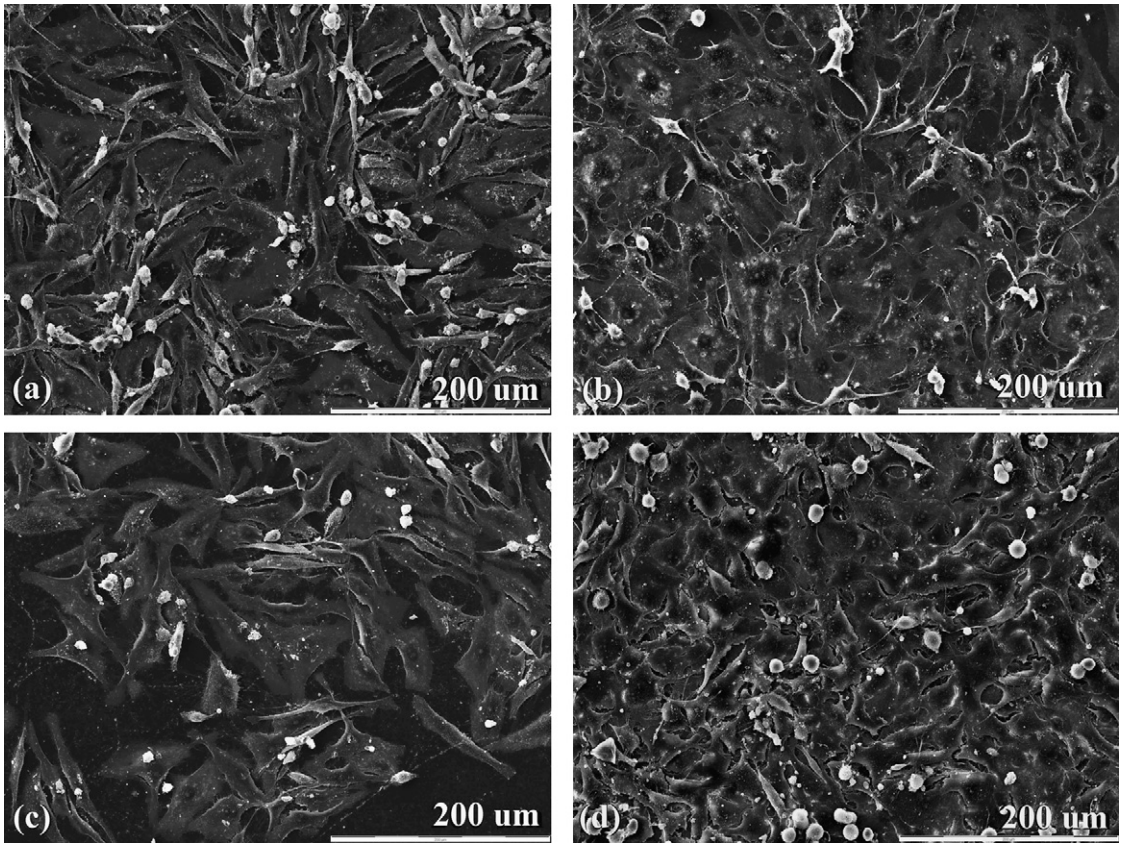

Fig. 6. SEM images of osteoblast-like cells incubated on HA grown on laser-treated (a and b) and non-treated (c and d) glass samples for 1 (a and c) and 3 (b and d) days.

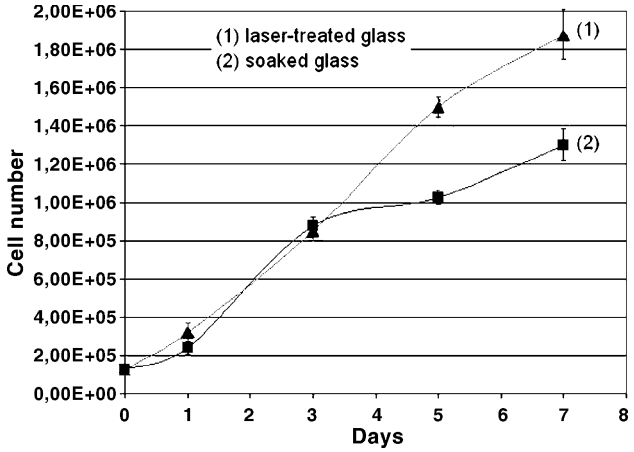

Fig. 7. Proliferation results show a permanent increase in the cell number on (1) laser-treated and (2) non-treated glass samples with increasing days of incubation.

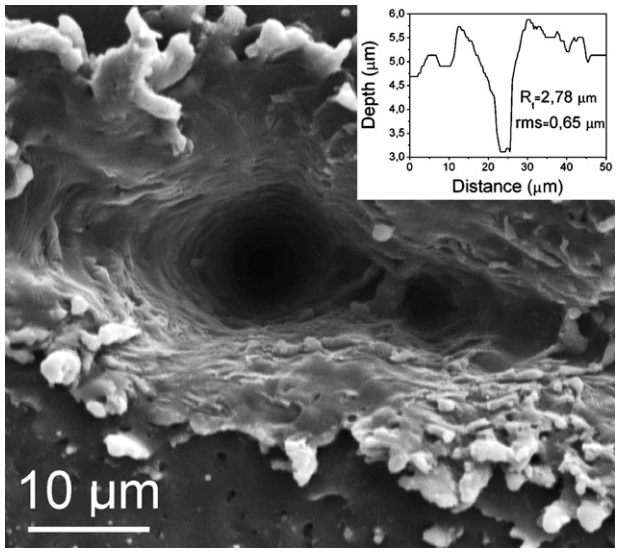

Fig. 9. SEM image of the Si surface after the end of the LLSI process reveals the formation of crater with corona structure at its edges due to melting and ablation. Inset shows the crater depth and rms roughness.

3.3. OES investigation during LLSI process

Up to now, a very limited number of works concerning 'laser–liquid–solid' interactions were published [52–57]. In the LLSI method utilized in our work, a complex interaction of the type 'laser–liquid–solid substrate' occurs. The surface of the materials after the LLSI process was observed by SEM and the image of the S surface is shown in Fig. 9. After the multi-pulse irradiation with the focused CuBr laser beam (power density was 60 MW/cm^2), the surface was locally melted and ablated, thus yielding the formation of a crater with corona structure at its edges. As estimated by CPM (inset profile in Fig. 9), the depth of the crater was 2.78 μm and the rms roughness measured over a line crossing the crater transversely was 0.65 μm. The shape of the crater was typical for a Gaussian beam profile in the focal point, as those used in our experiment. The same SEM images of crater formation were observed for the SS surface but the degree of melting and ablation was weaker. It is common in materials processing by high intensity nanosecond laser pulses that ablation occurs via extensive melting and evaporation [52–57]. In the applied power density range, plasma was formed and the molten material layer was pushed around the crater as a radial hydrodynamic flow due to the high recoil plasma pressures. Generally, mechanical irregularities introduced on the material surface are an advantage in the crystal growth processes because nuclei are easily attached to sites where surface defects exist [44]. This can explain the predominant attachment of CaP particles observed after the LLSI and revealed in Fig. 4a and b. Another advantage of the crater formation is the enlargement of the effective interfacial area of the materials. Mechanical roughness and high surface area are known to play a significant role in stable layer formation, and in anchoring cells and connecting together surrounding tissues, thereby leading to a shorter bone healing period. However, as a result of the ablation, rims are formed at the crater edge which is an inconvenient effect because the rims may break off the material surface during an implanting procedure and contaminate the surrounding biological tissues. Observation of the surface chemistry changes caused by the laser irradiation is a subject of a further study. Nonetheless, a decrease of the surface carbon contamination due to a cleaning effect of the laser beam, as well as surface oxidation is expected. Both are beneficial in facilitation the HA formation.

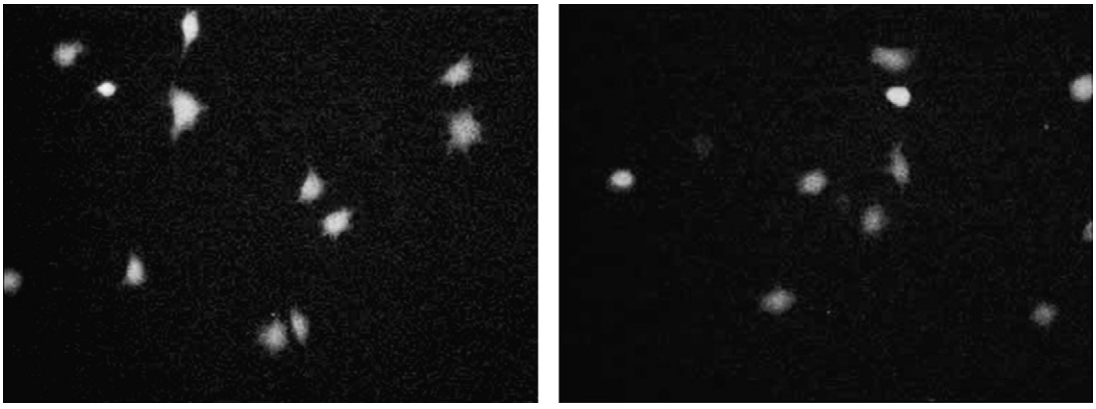

Fig. 8. Overall cell morphology of osteoblast-like cells adhering on laser-treated (left) and non-treated (right) glass samples.

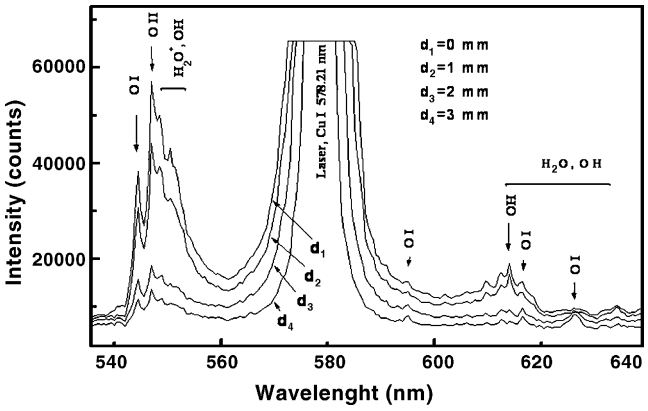

Fig. 10. Detailed optical emission spectra recorded during the LLSI process at different distances above the material–SBF interface.

OES technique was applied for the in situ monitoring of the processes during the LLSI process. The emission of visible light accompanying the laser pulses was collected at different positions starting from the material–SBF interface and going up to the SBF–air interface to study the expanding plasma. The strongest light emission was detected at the SBF–air interface. During the laser irradiation bubbles were observed to rise above the material surface. Optical emission spectra acquired in the SBF as a liquid, and at distances of 0 mm, 1 mm, 2 mm and 3 mm above the material–SBF interface are shown in Fig. 10. Peaks were identified using standard reference data tables [58], and the National Institute of Standards and Technology atomic spectra database [59]. The large peak in the centre was due to the scattered light from the laser main line at 578.2 nm. Peaks due to excited OH (553.06, 613.7, 623.58 and 625.8 nm) and H_2O molecule (616.57 and 618.15 nm) were detected in the detailed spectrum. Spectral lines of atomic oxygen O I (543.68, 595.83, 615.72 and 626.14 nm) and of ionized oxygen O II (546.10 nm) were also observed. Extended spectrum (not shown here) revealed additional peaks of hydrogen as follows: Hα at 656.27 nm, Hβ at 486.13 nm and Hγ at 434.049 nm, as well as He emission lines (He I at 388.86 and 447.14 nm) from the buffer gas used in the laser. Spectral lines of ionized oxygen O II at 708.39 nm and peaks in the range of 306.36–308.9 nm, at 312.17 and 347.21 nm assigned to OH molecule were detected. Because the intensity of the laser emission line was much stronger than those of the expanded plasma, large integration time was used. As a consequence, the second laser wavelength (510.6 nm) and the emission lines of He were present in the spectrum. At the chosen experimental conditions the emission lines of the SBF components were not observed. We consider that it will be necessary to acquire the emission signal from another direction allowing the lowest possible influence from the main laser line. In the present experiment, the acquiring direction was normal in respect to the laser beam as seen in Fig. 2. The formation of active species such as H_2O, OH, O and H can explain the high power of reaction of the plasma produced locally by the laser beam, and the possibility of CaP nuclei and particles formation just on the interaction point. Analyzing in detail the emission spectra shown in Fig. 10, an enhancement of the emission line intensity of oxygen was observed as the distance to the material–SBF interaction point decreased. This suggests a strong interaction of the laser beam with the atomic oxygen produced by the laser breakdown in the SBF, which led to the ionization of oxygen. We have to point out that the intensity of the oxygen lines increased only when the liquid was SBF, i.e. the presence of SBF as a liquid enhanced the production of oxygen. When distilled water was used as a control solution those line intensities were low and remained almost constant with increasing the distance from the material–SBF interaction point.

In summary, the interaction of the high intensity pulsed laser beam with the materials immersed in the aqueous solution (SBF) resulted in the formation of an ablation plume of ejected material in which the surface of the material and a small amount of the surrounding solution were vaporized to form bubbles within the solution. As more material was vaporized after the multiple pulses, the bubbles expanded, until at certain critical combination of temperature and pressure they collapsed. It is believed that at this point ionization and breakdown of SBF components within the bubbles could have occurred. We assume that in the LLSI process, the SBF solution trapped in the laser-induced bubbles instantly evaporated and resulted in the formation of CaP products. At the same time, the material surface was damaged and these CaP products immediately attached to the defect sites after the bubbles collapsed. Further nucleation was attained by diffusion of ions across the interfacial layer, assisted by the elevated temperature, and following supply of ions from the solution.

4. Conclusions

In this study we demonstrated a time-sparing method for the creation of surfaces organized on both micro- and nanoscale typical for nature, by simultaneously using a few stimuli (laser, solid surface and aqueous precursor solution). In the applied laser–liquid–solid interaction method, micrometer scale architecture with precisely controlled size and shape was induced by laser irradiation of various surfaces. Simultaneously with the employment of the laser–liquid–solid interaction in the SBF precursor solution, CaP particles and NaCl dendrites were formed during the laser irradiation time, which further facilitated the growth of a thicker carbonate-containing HA layer. Such fast CaP formation was not observed when the samples were simply soaked in the SBF. We consider that the few stimuli applied simultaneously, i.e. the solid surface, the laser beam and the aqueous precursor solution yielded a synergistic effect on the HA growth. Biocompatibility test with osteoblast-like cells revealed a good cell adhesion and spreading over the CaP layer grown on both laser-treated and non-treated glass samples, with more cells growing and proliferating on the laser-treated surfaces. Toxicity test showed cell viability on the two groups of samples of over 95%.

The new laser processing method can yield a significant progress in the materials coating with bone-like apatite in terms of nucleation rate, simplicity and availability to coat complex shapes. Since carbonate-containing HA is known as the major inorganic constituent of bones and teeth, the formation of such

material may have direct application in medicine, dentistry, and tissue engineering, particularly as the population ages.

Acknowledgements

This research was supported partly by the Bulgarian National Scientific Research Fund (grant L1213/02) and by the Eureka EU project (E!3033 Bionanocomposit, 2006/08). Short visits were supported through the bilateral agreements of the Bulgarian Academy of Sciences with the Hungarian and Romanian Academy of Sciences, as well as with Forschungszentrum Dresden-Rossendorf, Germany. We are grateful to Pulslight, Ltd., Sofia for the laser equipment and technical support. The assistance of E. Christalle, Dr. H. Reuther and Dr. A. Toth (SEM/EDX of HA layers), Dr. N. Shevchenko (XRD), Dr. P. Laquerriere (SEM of cells) and Prof. G. Altankov (LSCM of cells) is deeply acknowledged.

References

[1] J.C. Elliott, Structure and Chemistry of the Apatites and Other Calcium Orthophosphates, Elsevier Science, Amsterdam, 1994.
[2] B. Bunker, P. Rieke, B. Tarasevich, A. Campbell, G. Fryxell, G. Graff, L. Song, J. Liu, J. Virden, J. McVay, Science 264 (1994) 48–55.
[3] K. Polak, K. Sangwal, J. Cryst. Growth 152 (1995) 182–190.
[4] T. Kokubo, H. Kushitani, S. Sakka, T. Kitsugi, T. Yamamuro, J. Biomed. Mater. Res. 24 (1990) 721–734.
[5] Y. Fang, D. Agrawal, D. Roy, R. Roy, P. Brown, J. Mater. Res. 7 (1992) 2294–2298.
[6] T. Kasuga, H. Kondo, M. Nogami, J. Cryst. Growth 235 (2002) 235–240.
[7] E. Lerner, S. Sarig, R. Azoury, J. Mater. Sci. Mater. Med. 2 (1991) 138–141.
[8] L. Pramatarova, E. Pecheva, T. Petrov, N. Minkovski, A. Kondyurin, R. Pramatarova, Proc. SPIE 5449 (2004) 41–45.
[9] L. Pramatarova, E. Pecheva, T. Petrov, N. Minkovski, A. Kondyurin, R. Pramatarova, Proc. SPIE 5449 (2004) 46–50.
[10] L. Pramatarova, E. Pecheva, T. Petrov, A. Kondyurin, R. Pramatarova, N. Minkovski, Vacuum 76 (2004) 339–342.
[11] L. Pramatarova, E. Pecheva, D. Dimova-Malinovska, R. Pramatarova, U. Bismayer, T. Petrov, N. Minkovsky, Vacuum 76 (2004) 135–138.
[12] L. Pramatarova, E. Pecheva, R. Presker, M.T. Pham, M.F. Maitz, M. Stutzmann, Eur. Cells Mater. 9 (2005) 9–12.
[13] L. Pramatarova, E. Pecheva, D. Nesheva, Z. Aneva, A.L. Toth, E. Horvath, F. Riesz, Solid State Phenom. 106 (2005) 123–126 (from nanopowders to functional materials, edited by R. Piticescu, W. Lojkowski and J. Blizzard).
[14] C. Cotell, Appl. Surf. Sci. 69 (1993) 140–148.
[15] R. Narayan, Ch. Jin, A. Doraiswamy, I. Mihailescu, M. Jelinek, A. Ovsianikov, B. Chichkov, D. Chrisey, Adv. Eng. Mater. 7 (2005) 1083–1098.
[16] A. Richter, P. Gonprot, R. Smith, Methods Phys. Res. B 180 (2001) 1–11.
[17] G. Guzzardella, M. Fini, P. Torricelli, G. Giavaresi, R. Giardino, Lasers Med. Sci. 17 (2002) 216–220.
[18] A. Ebihara, B. Majaron, L.-H. Liaw, T. Krasieva, P. Wilder-Smith, Lasers Med. Sci. 17 (2002) 198–207.
[19] M. Kreisler, W. Kohnen, C. Marinello, H. Gotz, H. Duschner, B. Jansen, B. D'Hoedt, J. Periodont. 73 (2002) 1292–1298.
[20] A. Karacs, A. Joob Fancsaly, T. Divinyi, G. Peto, G. Kovach, Mater. Sci. Eng. C 23 (2003) 431–435.
[21] W. Lacefield, Materials characteristics of uncoated/ceramic-coated implant materials, presented at the 15th International Conference on Oral Biology (ICOB), Oral Biology and Dental Implants, Italy, Baveno 28 June–1 July, 1998.
[22] M. Long, H. Rack, Biomaterials 19 (1998) 1621–1639.
[23] I. Milosev, H. Strehblow, J. Biomed. Mater. Res. 52 (2000) 404–412.
[24] S. Anderson, H. Elliott, D. Wallis, L. Canham, J. Powell, Phys. Stat. Sol. A 197 (2003) 331–335.
[25] P. Siriphannon, Y. Kameshima, A. Yasumori, K. Okada, S. Hayashi, J. Biomed. Mater. Res. 52 (2000) 30–39.
[26] C. Wen, Y. Yamada, K. Shimojima, Y. Chino, H. Hosokawa, M. Mabuchi, Mater. Lett. 58 (2004) 357.
[27] C. Wilkinson, M. Riehle, M. Wood, J. Gallagher, A. Curtis, Mater. Sci. Eng. C 19 (2002) 263–269.
[28] A. Curtis, C. Wilkinson, Biomaterials 18 (1997) 1573.
[29] S. Bayliss, L. Buckberry, P. Harris, C. Rousseau, Thin Solid Films 297 (1997) 308.
[30] T. Webster, R. Siegel, R. Bizios, Biomaterials 20 (1999) 1221–1227.
[31] J. Coffer, J.-L. Montchamp, J. Aimone, R. Weis, Phys. Stat. Sol. A 197 (2003) 336.
[32] H. Wan, R. Williams, P. Doherty, D. Williams, J. Mater. Sci. Mater. Med. 8 (1997) 45.
[33] L. Suggs, M. Shire, C. Garcia, J. Anderson, A. Mikos, J. Biomed. Mater. Res. 46 (1999) 22.
[34] W. Chuang, T. Young, C. Yao, W. Chiu, Biomaterials 20 (1999) 1479.
[35] L. Pramatarova, E. Pecheva, Modified Inorganic Surfaces as a Model for Hydroxyapatite Growth, in Materials Science Foundations, vol. 26, Trans Tech Publications, Switzerland, 2006, pp. 1–122.
[36] D. Dimova-Malinovska, M. Kamenova, M. Sendova-Vassileva, Ts. Marinova, V. Krastev, Thin Solid Films 276 (1996) 248–252.
[37] D. Dimova-Malinovska, J. Optoelectr. Adv. Mater. 7 (2005) 99.
[38] W. Stumm, Aquatic Surface Chemistry: Chemical Processes at the Particle–Water Interface, Wiley XIX, New York, 1987, p. 228.
[39] R. Huddlestone, S. Leonard, Plasma Diagnostic Techniques, Academic Press, New York, 1965, p. 204.
[40] L. Clark, Mater. Today 2 (2000) 10–12.
[41] T. Tsuji, T. Kakita, M. Tsuji, Appl. Surf. Sci. 206 (2003) 314–320.
[42] D. Poondi, T. Dobbins, J. Singh, J. Mater. Sci. 35 (2000) 6237–6243.
[43] A. Simakin, G. Shafeev, E. Loubnin, Appl. Surf. Sci. 154-155 (2000) 405–410.
[44] B. Pamplin (Ed.), Crystal Growth, Pergamon Press, Amsterdam, 1980.
[45] R. LeGeros, J. LeGeros, Phosphate minerals in human tissues, in: J. Nriagu, P. Moore (Eds.), Phosphate Minerals, Springer Verlag, New York, 1984.
[46] R. LeGeros, Clin. Mater. 14 (1993) 65–88.
[47] R. Bube, Photoelectronic Properties of Semiconductors, Cambridge University Press, Cambridge, 1992.
[48] A. Angelescu, I. Kleps, M. Miu, M. Simion, C. Paduraru, S. Petrescu, V. Teodorescu, T. Neghina, A. Bragaru, Nanoscience & Nanotechnology, 4, Heron Press, Sofia, 2004, p. 285.
[49] L. Karlsson, P. Tengvall, I. Lundstrom, H. Arwin, Arwin, Phys. Stat. Sol. A 197 (2003) 326–330.
[50] S. Maendl, B. Rauschenbach, Surf. Coat. Technol. 156 (2002) 276–283.
[51] L. Pramatarova, E. Pecheva, P. Montgomery, D. Dimova-Malinovska, T. Petrov, A.L. Toth, M. Dimitrova, J. Nanosci. Nanotechnol., in press, doi:10.1166/jnn.2007.D163.
[52] D.A. Cremers, L.J. Radziemski, T.R. Loree, Appl. Spectrosc. 38 (1984) 721–729.
[53] Bundschuh, J.-I. Yun, R. Knopp, Fresenius J. Anal. Chem. 371 (2001) 1063–1069.
[54] R. Knopp, F.J. Scherbaum, J.I. Kim, Fresenius J. Anal. Chem. 355 (1996) 16–20.
[55] Koch, W. Garen, M. Müller, W. Neu, Appl. Phys. A 79 (2004) 1071–1073.
[56] M. Bereznai, I. Pelsoczi, Z. Toth, K. Turzo, M. Radnai, Z. Bor, A. Fazekas, Biomaterials 24 (2003) 4197–4203.
[57] E. Munoz, M. de Val, M. Ruiz-Gonzales, C. Lopez-Gascon, M. Sanjuan, M. Martinez, J. Gonzalez-Calbet, G. de la Fuente, M. Laguna, Chem. Phys. Lett. 420 (2006) 86–89.
[58] R.W.B. Pearse, A.G. Gaydon, Identification of Molecular Spectra, Chapman and Hall, Ltd., London, 1963.
[59] National Institute of Standards and Technology (NIST), http://www.nist.gov.